Clim Dyn
DOI 10.1007/s00382-014-2365-4

Partial lateral forcing experiments reveal how multi-scale processes induce devastating rainfall: a new application of regional modeling

Hongwei Yang · Bin Wang

Received: 5 June 2014 / Accepted: 6 October 2014

Abstract The 1998 extremely heavy rainfall events over East Asia are investigated through partial lateral forcing (PLF) experiments with the Weather Research and Forecasting model to determine the impacts of the synoptic (SY), intra-seasonal (IS), and inter-annual (IA) forcing across the lateral boundary on the extreme climate anomalies. The large-scale lateral boundary forcing was derived from an ensemble reanalysis dataset and decomposed into climatological, SY, IS, and IA components. The PLF experiments show that the IS forcing not only triggers the monsoon onset and drives two northward propagation events of the subtropical front but also has dominant contributions to the two heaviest rainfall events over the Yangtze River Basin (YRB) and South China, suggesting the critical role of the intra-seasonal variability in the devastating 1998 floods. Previous studies perceived that the northward propagating IS oscillation from the tropics regulates the extreme heavy rainfall of East Asia summer monsoon in 1998. However, we find that the IS forcing from the mid-latitude plays a more important role than the forcing from the tropics in generating the two extreme rainfall events in 1998. During the first extreme event in June, the IS forcing across the western boundary is the major cause of the northward advance of the subtropical front and the heavy rainfall over the YRB and South China, with the IS forcing across the northern boundary providing the second largest contribution. During the second extreme event (July 15–August 5), the IS forcing from the eastern boundary plays a dominant role in driving the southward retreat and northward advance of the subtropical front, causing another heavy rainfall over the YRB and South China. The western and northern IS forcing also has large contributions to the second extreme event. We have estimated the contributions to the seasonal anomalous rainfall by the three types of forcing. The SY forcing tends to have a moderate effect on the YRB rainfall but significant reduction of the rainfall in South China. The IS forcing has dominant contributions to the seasonal-mean rainfall anomalies over all three subregions of China (North China, the YRB, and South China). The IA forcing mainly enhances the rainfall in South China but reduces the precipitation in the YRB slightly. This study portends a promising application of regional climate models to identify key factors causing extreme climate events. The PLF methodology can be used to study a broad range of climate phenomena and to understand the effects of variety of dynamic and physical processes in climate variability and predictability.

Keywords Partial lateral forcing · Monsoon dynamics · Synoptic disturbance · Intra-seasonal oscillation · Inter-annual variation · Extreme rainfall

H. Yang (✉)
APEC Climate Center, Busan, South Korea
e-mail: hwyangapcc@gmail.com

B. Wang
Department of Meteorology and International Pacific Research Center, University of Hawaii at Manoa, Honolulu, HI, USA

B. Wang
Earth System Modeling Center/NIAMS, Nanjing University of Information Science and Technology, Nanjing 210044, China

1 Introduction

Heavy rainfall during East Asia summer monsoon (EASM) season has considerable societal impacts on the most populated area in the world. The onset of the EASM begins with the establishment of the westerlies

Published online: 21 October 2014

and rainy season over the South China Sea (SCS) around mid-May. As the summer monsoon develops, the East Asia subtropical front and associated rain band migrate northward. Around June 10, the monsoon rain band moves over the Yangtze-Huaihe River Basin, which marks the beginning of the Meiyu season in China (Ding 1994; Wang and LinHo 2002). The Meiyu reaches its peak in late June. The rain band advances to northern China in July and finally retreats from northern China in late August. Detailed description about the EASM can be found in Ding (1994) and Chang (2004).

Two devastating flooding episodes occurred in the Yangtze River Basin (YRB) and South China in summer 1998. The first occurred during a normal Meiyu period in June, whereas the second occurred during the climatological dry period of the YRB in mid-July to early August. The "double" Meiyu peaks caused the most devastating flooding in the YRB since 1954. The flooding caused 166 billion RMB in damages according to National Climate Center of China (NCC 1998). More information on the flooding can be found in Ding and Liu (2001) and Wang et al. (2003).

The climate background of the 1998 flooding was unique. During winter 1997/1998, the strongest El Nino in the twentieth century (McPhaden 1999) enhanced the East Asia precipitation over the Tibetan Plateau and South China, which resulted in deepened and extended snow cover over the Tibetan Plateau and increased soil moisture in South China (Tao et al. 1998). The extensive snow that persisted until spring 1998 weakened the EASM due to reduced large-scale thermal contrast between the Asian land mass and Pacific Ocean. The rain band in this weak EASM season shifted southward and concentrated over the YRB instead of moving farther north as it would during normal and strong EASM years (Tao et al. 1998; Chen 2001). On the other hand, the saturated underlying soil in South China favored excess runoff in the coming Meiyu season.

Accompanied with the El Nino development, an anomalous high pressure originated near Philippine during autumn 1997 developed into its peak phase during early spring of 1998 (Wang and Zhang 2002). The anomalous western Pacific subtropical high (WPSH) and the underlying sea surface temperature (SST) cooling to its southeast maintained themselves well into summer 1998, due to a positive thermodynamic feedback between the two (Wang et al. 2000a; Lau et al. 2005). In summer 1998, the anomalous WPSH enhanced the southwesterly monsoon, and moisture converged in the YRB. In addition, two intraseasonal (IS) oscillation events had propagated northward from the SCS to 30°N–35°N (Tao et al. 1998; Wang et al. 2003; Zhu et al. 2003; Lu et al. 2014), which regulated the monsoon strength and the associated rainfall (Goswami et al. 2006). Furthermore, the blocking high over the Ural Mountains and the Okhotsk Sea in June and July and that over the Lake Baikal in August occurred more frequently (NCC 1998). The southern branch of the cold air split by the blocking high pushed the mid-latitude front southward farther than normal to the YRB (Wang 2006). Low-level vortices from the southeastern Tibetan Plateau actively migrated eastward (Ding et al. 2001). Finally, the summer tropical SST anomaly is also important to cause the heavy rainfall in 1998 (Wang et al. 2000b). The combined effects of synoptic (SY) disturbance, IS oscillation, and inter-annual (IA) variation resulted in the devastating 1998 flooding in East Asia.

More than 15 years later, however, interesting questions remain as to what really dominated the extreme heavy rainfall events in the YRB and South China in summer 1998. How did the large-scale forcing influence the EASM in 1998? We are motived to address those questions here through the partial lateral forcing (PLF) experiments with the Weather Research and Forecasting (WRF) model (Skamarock et al. 2005). Briefly, we decomposed the lateral boundary (LB) forcing of the WRF model into the external SY, IS, and IA components and performed a suite of sensitivity experiments. The influence of each external forcing can be identified by comparing the sensitivity experiment with the control run.

We introduce the model, setup of the PLF experiments, and how to extract the SY, IS, and the IA signals from the LB forcing in Sect. 2. The results are described in Sects. 3–6. The conclusion and discussion are given in Sect. 7.

2 Methodology

2.1 Decomposition of the lateral boundary forcing

The decomposition of the variables used at the LB was conducted as follows.

First, the climatological annual cycle (AC) was obtained by calculating 31-day running mean over the climatological daily mean data averaged for the period from 1979 to 2001 in the 365-day calendar.

Second, the daily mean anomaly was obtained by subtracting the AC from the daily mean data. The IA component was further obtained by calculating 365-day running mean over the daily mean anomaly data.

Finally, the (SY + IS) field was obtained by subtracting the IA component from the daily mean anomaly data. The IS component was further separated from the SY component by calculating 5-day running mean over the (SY + IS) field.

Through the above three steps, the SY, IS, and the IA variations of humidity, temperature, horizontal winds, and geopotential height of the large-scale forcing were obtained.

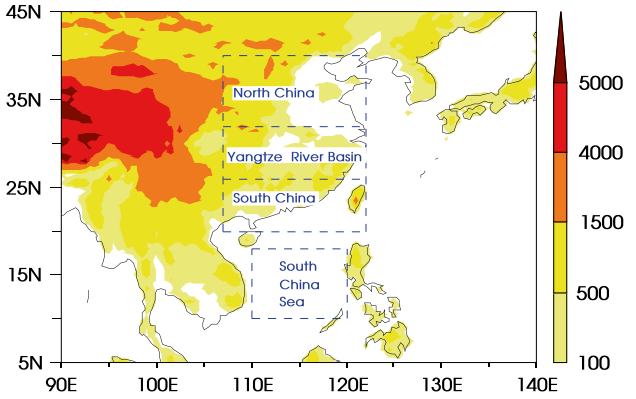

Fig. 1 Model domain and topography (*color shadings* in units of meters). Topographic *contours* of 1,500, 4,000 and 5,000 m are highlighted. The *rectangular boxes* marked by *dashed blue lines* refer to the following regions: the central South China Sea (10°N–18°N, 110°E–120°E), South China (20°N–26°N, 107°E–122°E), the Yangtze River Basin (YRB; 26°N–32°N, 107°E–122°E), and North China (32°N–40°N, 107°E–122°E)

2.2 Experimental design

The model domain covers the region from 5°N to 45°N and from 90°E to 140°E. The Mercator map projection is adopted. The zonal grid space is precisely 0.5° and the meridional grid space is approximately 0.5° with a slight northward reduction; so the model has 92 meridional and 101 zonal grid points. There are 31 sigma levels in the vertical direction. The topography map (Fig. 1) shows that the steepest slopes are located south and east of the Tibetan Plateau.

Wang and Yang (2008) carried out a dynamical downscaling study of the EASM in 1998 using the WRF model. In that study, the WRF model realistically reproduced the seasonal-mean precipitation, seasonal march of the Meiyu rain band, and daily rainfall events in the five-member control experiment (CTL) forced by the ensemble mean of reanalysis dataset from the National Centers for Environmental Prediction/Department of Energy (R2; Kanamitsu et al. 2002) and the reanalysis dataset from the European centre for Medium-Range Weather Forecasts 40-year reanalysis (ERA40; Uppala et al. 2005). We use the member of that CTL experiment initiated at 12Z April 24, 1998 in Wang and Yang (2008) as the CTL experiment in this study. The forcing fields include air temperature, specific humidity, zonal and meridional winds, and geopotential height at standard pressure levels, which were interpolated to match the regional model's resolution. The surface initial conditions included surface pressure, sea-level pressure, temperature and moisture at 2-m height, skin temperature on the land surface, horizontal winds at 10-m height, water equivalent of snow depth, soil moisture, and soil temperature. The skin temperature over the ocean is considered as SST. Interested readers may refer to Wang and Yang (2008) for assessment of their CTL experiment.

To study the effects of the SY, IS, and the IA variations in the LB forcing on the EASM, we designed the PLF experiments; first four experiments are named as Exp_noSY, Exp_noIS, Exp_noIA, and Exp_noSYISIA, in which the SY, IS, IA, and their sum are respectively taken out from the LB forcing. The initial values at the surface in the four experiments are kept the same as in the CTL experiment, whereas on each pressure level the corresponding SY, IS, IA, and their total sum are separately taken out from the total fields of the initial variables.

To identify the role of the IS forcing across each sides of the LB, the IS forcing is separately taken out from the eastern, southern, western, and northern LB forcing in additional four PLF experiments based on the CTL experiment, and were named as Exp_EnoIS, Exp_SnoIS, Exp_WnoIS, and Exp_NnoIS, respectively.

In all the experiments, the days before May 1 are considered as the "spin-up" period. The outputs from May 1 to August 31 are analyzed. The physical parameterizations and model configuration are kept the same for all the experiments.

3 Impacts of multi-scale forcing on seasonal mean precipitation anomalies

Figure 2 shows the impacts of different time-scale forcing on seasonal-mean (June–August or JJA) circulation and precipitation as measured by the difference maps between the CTL and sensitivity experiments (Exp_noSY, Exp_noIS, Exp_noIA). The impacts are also compared with the anomalies derived from observation and the ensemble reanalysis.

Figure 2a shows that a significant positive height anomaly occupied a large area include the entire tropical region indicates the stronger WPSH and moisture convergence over the YRB in summer 1998 relative to the normal years. Figure 2b shows that significant positive rainfall anomalies were located over the YRB, which are partly overlapped by a significant positive vorticity anomaly occurred over a large area along the subtropical frontal zone tilted southwest-northeast from South West China to the Korean peninsula. In contrast, a significant negative vorticity anomaly occurred over most tropical areas.

The eastward moving low-pressure disturbance from the Tibetan Plateau is one of the main SY signals over East Asia. Figure 2c, d indicate that the LB SY forcing from outside of the domain induces a significant positive height anomaly centered on the Korea Peninsula (Fig. 2c), which is collocated with significant negative anomalies in precipitation and low-level vorticity (Fig. 2d). The LB SY forcing

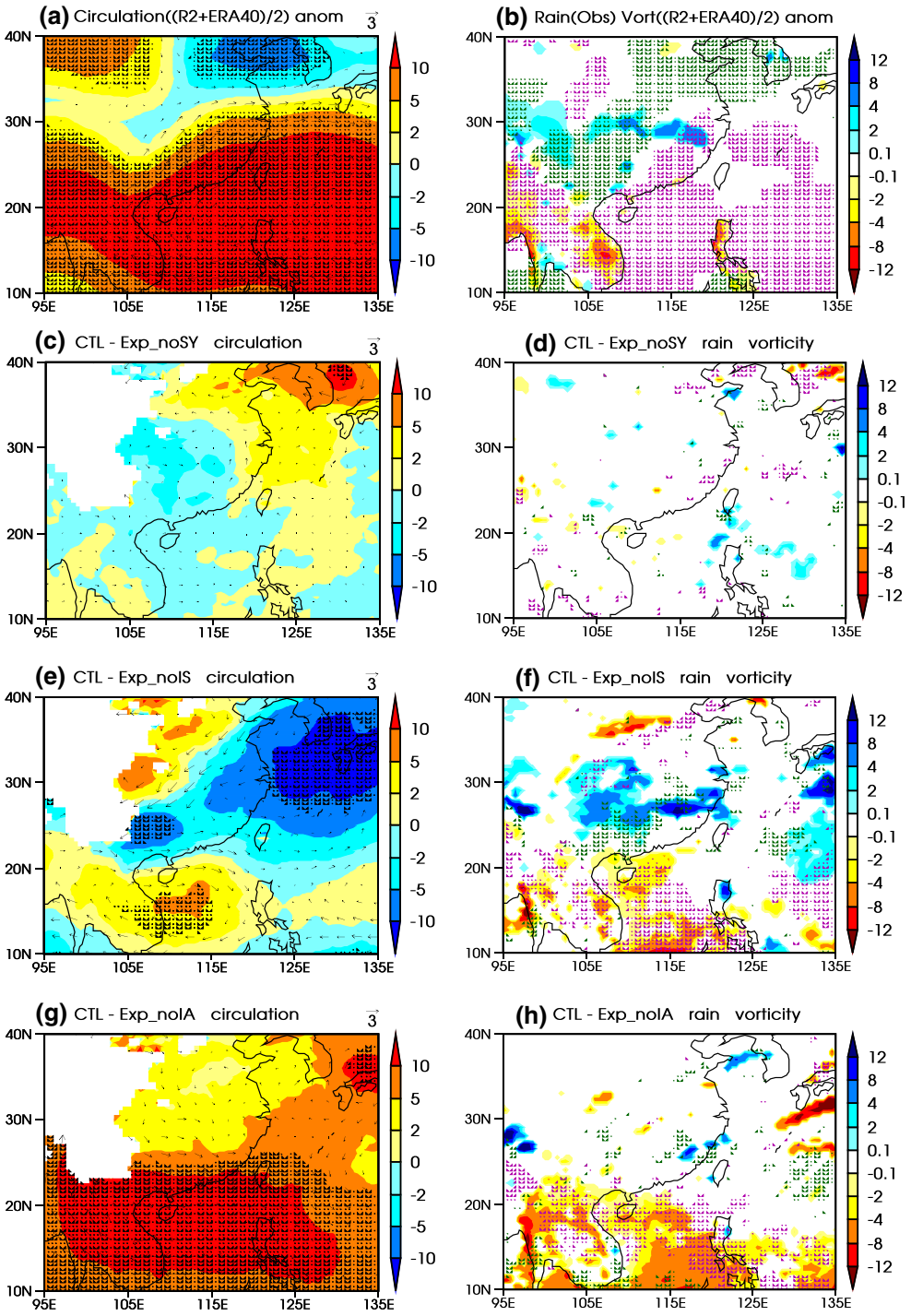

Fig. 2 Impacts of multi-time scale forcing on seasonal-mean anomalies. **a** Anomalous geopotential height and horizontal wind of the ensemble reanalysis on 850 hPa in JJA. **c**, **e** and **g** Show differences in geopotential height and horizontal wind on 850 hPa in JJA between the CTL and the sensitivity experiments of Exp_SY, Exp_IS, and Exp_IA, respectively. Geopotential height is shaded in units of meters and vectors present horizontal wind in units of m s^{-1}. *Black hatching* indicates the area where the geopotential height is significantly changed. **b** Shows significant anomalies in observed rainfall (Yatagai et al. 2009) and 850-hPa vorticity of the ensemble reanalysis in JJA. **d**, **f** and **h** Show significant differences in rainfall and 850-hPa vorticity in JJA between the CTL and the three sensitivity experiments. Rainfall is shaded in units of mm day^{-1}. *Green* (*pink*) *hatching* indicates the area where the anomalous vorticity is positive (negative). The anomalies of the ensemble reanalysis and observed rainfall are derived from the data between 1979 and 2001. All significance areas are at the 95 % confidence level by the *t* test

significantly increases the precipitation and low-level vorticity around the southern tip of Taiwan (Fig. 2d). However, the SY forcing does not show organized impacts on precipitation and vorticity over other regions.

The external IS forcing produces much stronger rectifications to the seasonal-mean fields than the SY forcing does. The IS forcing significantly lowers geopotential height over the East China Sea, South Korea, and western Japan (Fig. 2e) as well as in South China; meanwhile it increases the height over the SCS and Indochina Peninsula which significantly contributes to the observed anomalous height (Fig. 2a). The IS forcing enhances the rainfall over the lower reaches of YRB and a large area of Central China (Fig. 2f) where the significant wet anomalies was observed (Fig. 2b). The significantly increased positive low-level vorticity is collocated with the enhanced rainfall along

the subtropical frontal zone tilted southwest-northeast over the YRB (Fig. 2f) which significantly contributes to the positive anomalous vorticity in the ensemble reanalysis (Fig. 2b). The coherence of the heavy rainfall centers among the observation (Fig. 2b), the CTL, and the difference of CTL from Exp_noIS (Fig. 2f) indicates the IS forcing was a main cause for the extreme heavy rainfall in summer 1998. Nevertheless, the wet anomaly also appears over parts of the western North Pacific and Tibetan Plateau, and most of those seasonal wet conditions are collocated with significantly increased positive vorticity (Fig. 2f). In contrast, significant dry conditions and negative vorticity anomaly are found over most tropical areas, and along a narrow band in North China, which is coherent with the significant negative vorticity anomaly in the ensemble reanalysis (Fig. 2b).

The IA forcing results in a positive anomalous height over the entire tropical area in the model domain, and a small region over Japan (Fig. 2g), where negative precipitation anomaly and vorticity anomaly are seen (Fig. 2h). Those positive height anomaly, negative precipitation anomaly, and negative vorticity anomaly over tropical regions contributes largely to the anomalies of observation and the ensemble reanalysis (Fig. 2a, b). On the other hand, similar to the effect of the IS signal discussed earlier, the IA forcing also significantly enhances the precipitation and the positive vorticity over the lower reaches of YRB (Fig. 2h). The in-phase effects of IS and IA forcing on precipitation lead to the extreme flooding over the YRB. Other regions with significantly increased precipitation and positive vorticity include the Tibetan Plateau and the Yellow Sea. The later may cause flooding over the Korean Peninsula (Fig. 2b).

In term of seasonal-mean climate, the external IS forcing contributes most to the heavy rainfall over South China and the YRB while it suppresses rainfall over North China and the tropical monsoon trough region in the western Pacific.

As a rough estimate, we computed the contribution of each forcing to the seasonal-mean precipitation anomaly averaged over three sub-regions of China, namely, North China, the YRB, and South China (Fig. 1). We estimated these contributions using the differences between the CTL and the no-forcing experiment (Exp_noSYISIA). Note that due to nonlinear effects, this linear estimation does not yield precisely balanced percentage contributions, but it does offer, in a quantitative sense, the relative importance of different time-scale forcing on the precipitation anomalies in the three sub-regions of China. For North China, the SY, IS, and IA contributions are 5, 81 and 16 %, respectively. For the YRB, the SY, IS, and IA contributions are approximately 16, 107, and −14 %, respectively. For South China, the SY, IS, and IA contributions are −47, 125, and 56 %, respectively. Overall, the SY forcing tends to have a moderate positive contribution to the YRB but significant negative contribution to the rainfall in South China. The IS forcing has the largest contributions to the seasonal-mean rainfall anomalies over all three sub-regions of China. The IA forcing mainly enhances the rainfall in South China but reduces the rain in the YRB slightly.

4 Impacts of multi-scale forcing on migration of subtropical front

To investigate the temporal evolution of the East Asia subtropical front and its associated rain band, we examine daily outputs and display the results by means of the hovmoller diagram using the low-level vorticity at 850 hPa averaged along the longitude band between 107°E and 120°E. The low-level vorticity band represents the subtropical front and its associated precipitation band very well. In the following discussion, the positive vorticity anomaly will also be alternatively interpreted as positive rainfall anomaly and/or enhanced frontal zone.

In summer 1998, there were two northward migration events of the frontal zone based on the ensemble of reanalysis datasets (Fig. 3a). The first event started from mid-May to the end of May, with suddenly increased rainfall over the SCS indicating the monsoon onset (Wang et al. 2004). The frontal zone and rain band then marched northward from about 20°N in early June to around 40°N in mid-July (Fig. 3a), bringing huge amount of rainfall to South China and the YRB. For convenience, we name this as the first flooding period (FLOOD1). Starting from mid-July, the subtropical front suddenly retreated to the YRB and produced another severe rainfall event during late July to early August, which worsened the local flooding. We name this as FLOOD2. During FLOOD2, the subtropical front moved slowly northward until late August (Fig. 3a).

Figure 3b shows that the CTL reproduces realistically the observed movement of the subtropical front, including the SCS monsoon onset, the northward migration of the rain band during FLOOD1, the sudden retreat of the frontal zone in mid-July, and the slow northward propagation of the frontal zone during FLOOD2.

Figure 3c, d show the hovmoller diagrams of vorticity in Exp_noSY and its departure from the CTL. The latitude-time pattern of vorticity in Exp_noSY (Fig. 3c) is similar to that in the CTL (Fig. 3b), suggesting that the SY forcing does not significantly affect the northward migration of the rain band except that many vorticity disturbances are generated by the SY forcing, and strong disturbances occasionally break the northward migration of the vorticity associated with the subtropical front. The disturbances show strong spatial–temporal variability in the area on the north side of the subtropical front (Fig. 3d). Generally, the

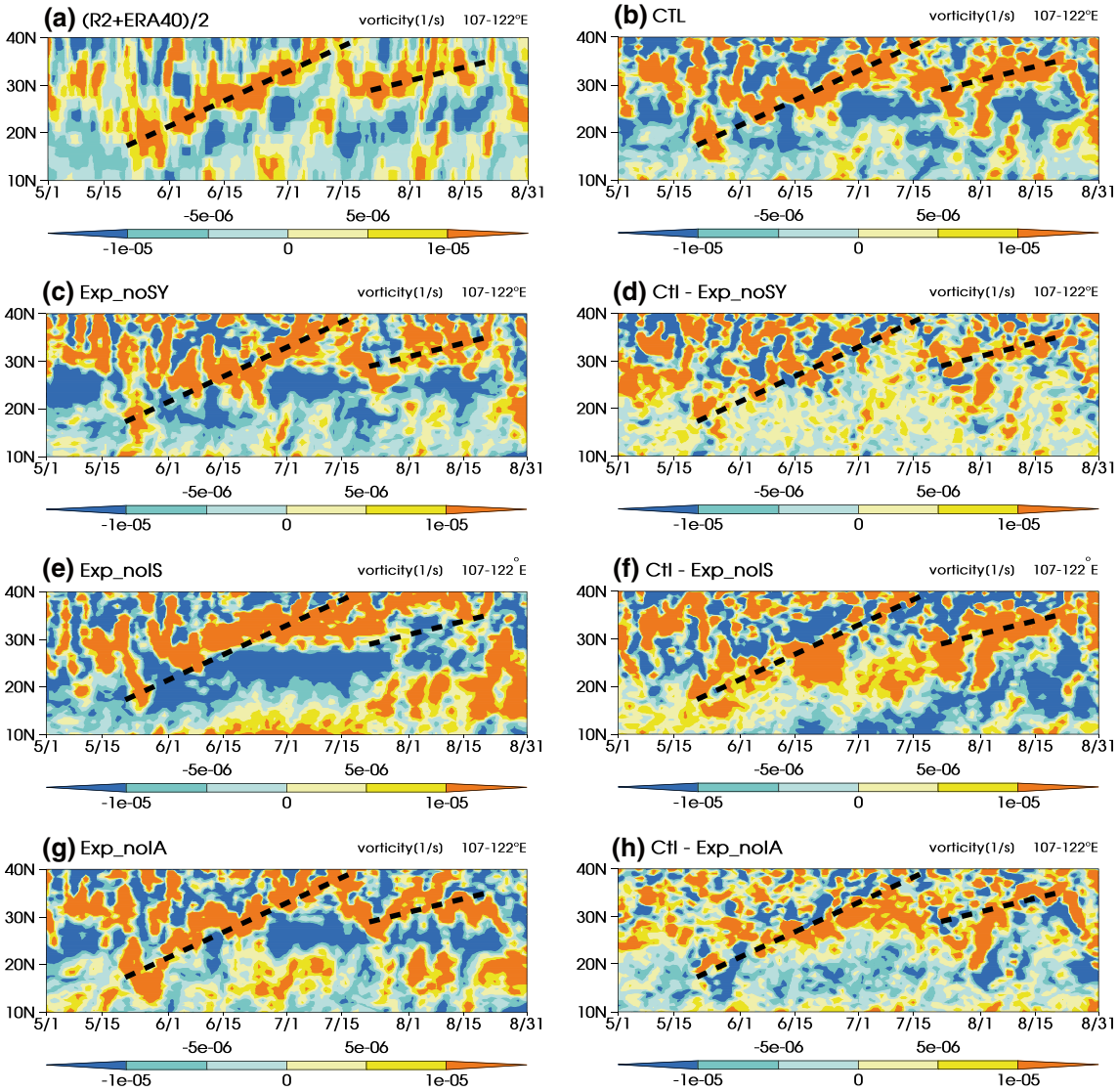

Fig. 3 Time-latitude cross sections of daily vorticity (s^{-1}) on 850 hPa in eastern China averaged between 107°E and 122°E from May 1 to August 31, 1998, which are derived from **a** ensemble reanalysis, **b** CTL, **c** Exp_noSY, **e** Exp_noIS, and **g** Exp_noIA. **d**, **f** and **h** are the differences of **b** with respect to **c**, **e** and **g**, respectively. These difference maps show the influences of the SY, IS, and the IA forcing on northward propagation of the front and heavy rainfall events, respectively. *Dashed lines* indicate the twice northward propagating path of vorticity in FLOOD1 and FLOOD2

interruption of the positive vorticity anomalies is relatively less in FLOOD2 (Fig. 3d), which may suggest an enhancement of the local rainfall.

The hovmoller diagram of Exp_noIS (Fig. 3e) exhibits remarkably different northward migration pattern of the subtropical front from that in the CTL (Fig. 3b). The positive vorticity during FLOOD1 starts at a location north of that in the CTL at the beginning of June, and it stays around the same latitudes until mid-July with a very slow and inevident northward propagation (Fig. 3e). The retreat of the subtropical front during July 15 and August 1 in the CTL is missing from Exp_noIS (Fig. 3e). The second northward migration of the subtropical front shifts much too north and appears to be a continuation of the first event, which moves toward north from mid-July to mid-August (Fig. 3e). Meanwhile, high-frequency positive SY vorticity propagates northward over the SCS. This synoptic regime gradually shifts northward, passes the southern coastline, and invades South China after July 20 and then the YRB.

The effect of the IS forcing can be seen more clearly from the difference of CTL minus Exp_noIS (Fig. 3f). The positive vorticity anomalies are pronounced over the SCS in late May, suggesting that the IS forcing plays an essential role in triggering the EASM onset. Around June 15 between

20°N and 30°N, a positive vorticity anomaly occurs over a large latitudinal extent during the second half of June. This anomaly corresponds to the extreme heavy rainfall in FLOOD1 over the YRB and South China. After July 1, this anomaly suddenly weakens but still intermittently moves toward 40°N until July 15. Meanwhile, another positive vorticity anomaly forms around 20°N on July 1 and intensifies over a large area when it reaches 30°N around July 20, suggesting the important contribution of the IS forcing in sustaining FLOOD1. Also notable is FLOOD2, which almost entirely attributes its existence to the IS forcing. Thus, the heavy rainfall over South China and the YRB during FLOOD2, and the enhanced rainfall over North China in August are largely linked to the IS forcing. These distinctive features of the EASM flooding in 1998 would not have existed if the external IS forcing were absent (Fig. 3e).

The hovmoller diagram of vorticity in Exp_noIA (Fig. 3g) is similar to that of the CTL (Fig. 3b), suggesting that the IA forcing plays a minor role in the two northward propagation events. In fact, for the first northward migration of the positive vorticity anomaly, the IA forcing tends to shift the anomaly southward during the period from June 15 to early July (Fig. 3h), indicating its negative contribution to the northward propagation. Around July 7, it begins to cause excessive rainfall in the YRB, which is much earlier compared with the corresponding retreat of the subtropical front in the CTL (Fig. 3b). Overall, the IA forcing does not have a positive contribution to the two northward propagation events in July and early August.

To sum up, the external IS forcing is the major trigger of the SCS monsoon onset. Both extreme heavy rainfall events are dominated by the IS forcing. Both SY forcing and IA forcing enhance the positive vorticity in FLOOD2, but their contributions are less important compared with that of the IS forcing. The two northward propagating events outlined in Fig. 3 are primarily caused by the IS forcing, with little contributions from the SY and IA forcing.

5 Effects of multi-scale forcing on extreme rainfall events

In this section, we focus on the two extreme events and examine the impacts of the three individual forcing (SY, IS, and IA).

The areal-averaged daily rainfall evolution in Fig. 4 clearly shows the effects of the SY, IS, and IA forcing on the extreme rainfall events over North China, the YRB, and South China. The background grey arrows in Fig. 4 mark the two northward migration events of the subtropical front and the sudden retreat in between in the CTL. The extreme rainfall events in June through August take place upon the arrival of the subtropical front. FLOOD1 in June corresponds to the background arrow on the left in Fig. 4. FLOOD2 in late July and early August corresponds to the middle and right background arrows in Fig. 4. If the CTL produces more precipitation than a sensitivity experiment, the area between the two precipitation curves is filled with light blue color; otherwise, it is filled with light brown color. For example, in the case of Exp_noSY (Fig. 4a), the light blue color indicates reduced rainfall when the external SY forcing is removed. In other words, the light blue color means the positive contribution of the SY forcing to the rainfall field in the CTL.

Figure 4a shows that along with the first northward migration of the subtropical front, the SY forcing does not influence FLOOD1 remarkably, except for its contribution to the maximum rainfall intensity over the YRB around June 20. The effect of the SY forcing is negligible during the retreat of the subtropical front. However, the SY forcing starts to enhance rainfall over South China and pushes the enhancement northward to the YRB during the second northward march of the subtropical front; so it contributes moderately to FLOOD2.

Figure 4b shows that the IS forcing dramatically increases rainfall to FLOOD1 over South China and the YRB during the first northward migration of the subtropical front. Around July 15, the subtropical front suddenly retreats to the YRB and then to South China, which significantly worsens the flooding situation. Finally, the rain band returns northward back to the YRB and North China. The IS forcing brings a huge amount of rainfall to the YRB as well as South China during the FLOOD2.

Figure 4c shows that the IA forcing contributes little to FLOOD1. However, it enhances the rainfall over South China when the subtropical front retreats in mid-July. Later, the enhanced rainfall moves northward to the YRB along with the subtropical front. Thus, the IA forcing has a considerable contribution to FLOOD2.

Figure 4 demonstrates that the IS forcing contributes most to the severe flooding over the YRB and South China during both FLOOD1 and FLOOD2. The SY forcing and IA forcing enhance the precipitation over the YRB and South China mainly during the second northward propagation of the subtropical front (late part of FLOOD2). When the subtropical front retreats from North China in mid-July (the early part of FLOOD2), the IS forcing brings a large amount of rainfall to the YRB, while the SY forcing and IA forcing have little contribution.

6 Sources of intra-seasonal forcing that influence the extreme rainfall events

The numerical experiments and analysis so far have shown that external IS forcing not only triggers the SCS monsoon

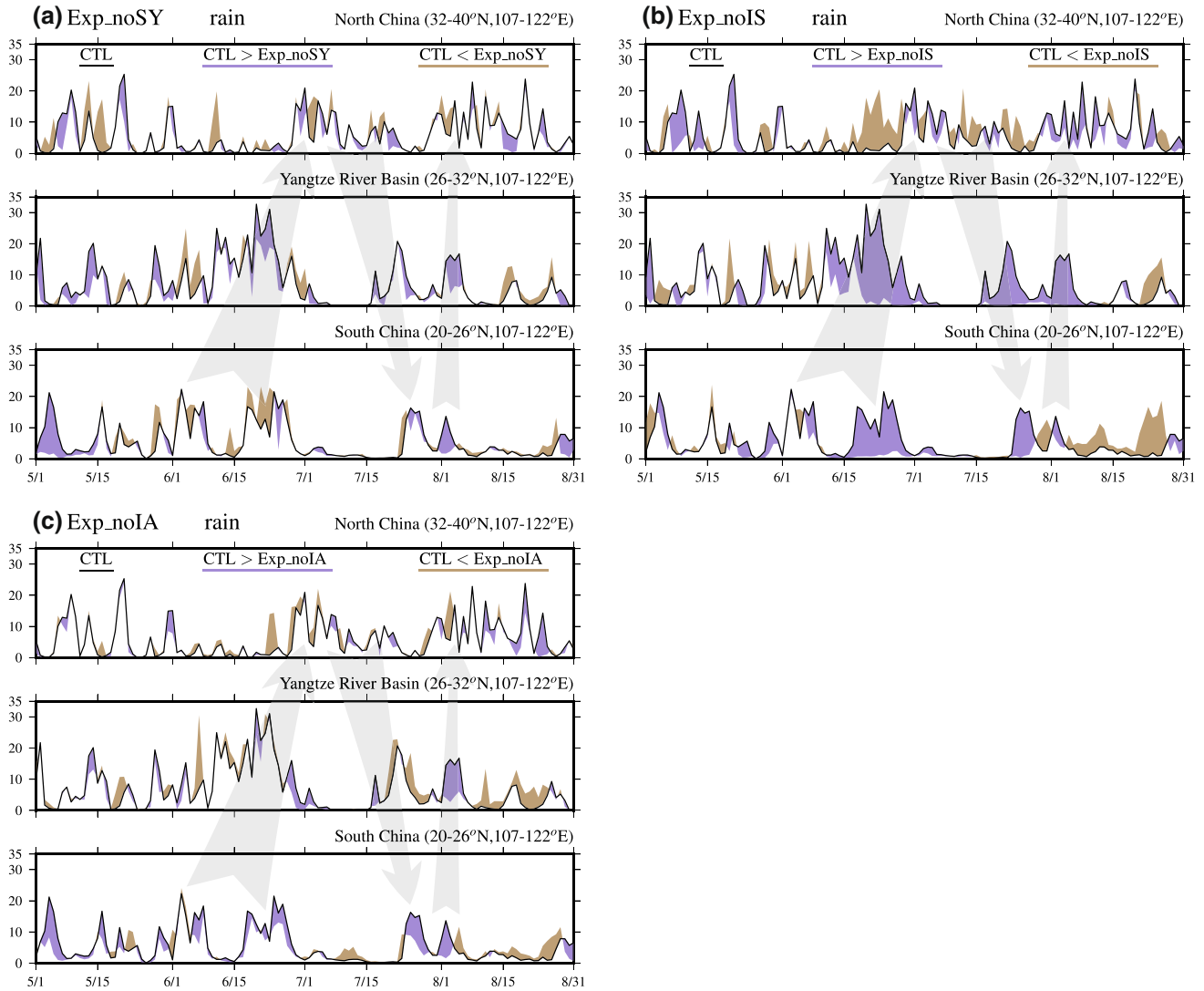

Fig. 4 Impacts of multi-time scale forcing on extreme rainfall events. The area-averaged daily precipitation rates (mm day^{-1}) over land in the CTL (*solid black curve*) and its differences (*colors*) from the sensitivity experiments of Exp_noSY, Exp_noIS, and Exp_noIA in (**a**–**c**), respectively. *Light blue* (*light brown*) *color* indicates that the precipitation in the CTL is larger (less) than that in the sensitivity experiment. The wide *grey arrows* indicate the two northward marches of the subtropical front and one retreat in between

onset, but also dominates the northward migration of the subtropical front and the two heavy precipitation events that lead to the flooding disaster over the YRB and South China. We are motivated to investigate where the IS forcing came from, the tropics or the mid-latitude in this section. Specifically, we use four sensitivity experiments of Exp_WnoIS, Exp_EnoIS, Exp_SnoIS, and Exp_NnoIS to examine the impact of the IS forcing through each of the four LBs.

Figure 5a shows the effects of the IS forcing from the western boundary (western IS forcing), with light blue (light brown) color representing positive (negative) rainfall contribution. Obviously, the western IS forcing enhances the subtropical front and the associated extreme rainfall during both FLOOD1 and FLOOD2. Similar to the effects of the total IS forcing, the western IS forcing enhances the heavy rainfall with a broad scale that lasts more than 10 days over both South China and the YRB during FLOOD1. Different from the total IS forcing, the western IS forcing contributes less amount of rainfall when the subtropical front retreats to the YRB.

Figure 5b shows that the northern IS forcing has a moderate contribution to the enhancement of the rainfall during FLOOD1, especially in mid-June over the YRB. The northern IS forcing seems to have a significant contribution to increased rainfall over all three sub-regions (North China, the YRB, and South China) during FLOOD2, especially when the subtropical front retreats southward.

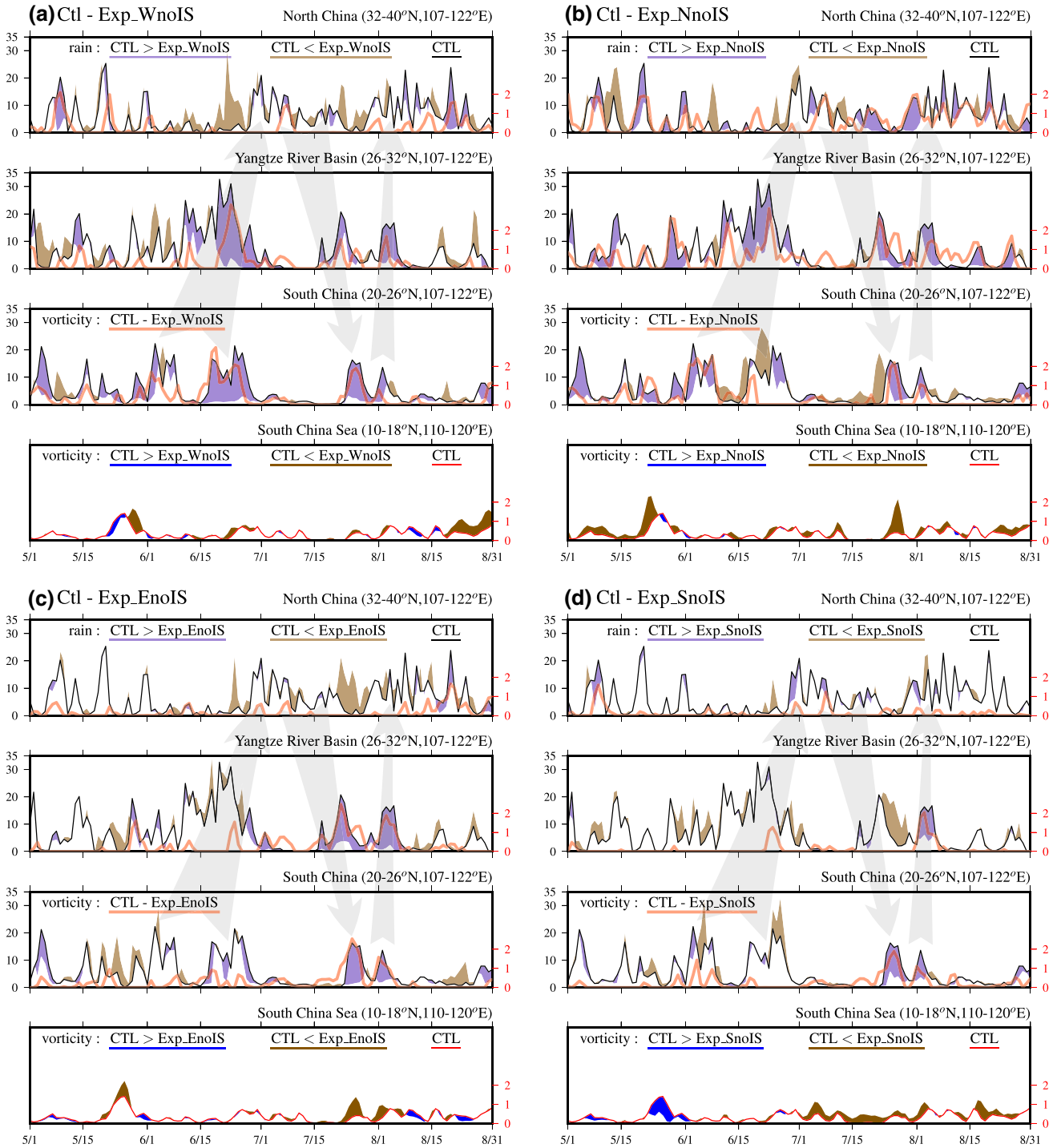

Fig. 5 Impacts of different sources of IS forcing on the heavy rainfall events. The first three panels of (**a**–**d**) blocks show area-averaged daily precipitation rates (mm day^{-1}) over land in the CTL (*solid black curve*) and its differences (*color*) from the sensitivity experiments of Exp_WnoIS, Exp_NnoIS, Exp_EnoIS, and Exp_SnoIS over North China, the YRB, and South China, respectively. *Light blue* (*light brown*) *color* indicates that the precipitation in the CTL is larger (less) than that of the sensitivity experiment. *Thick pink curve* is the difference of area-averaged daily positive vorticity of the CTL with respect to each sensitivity experiment over land. The last panel in each block is the area-averaged daily positive vorticity (1E−5 s^{-1}) in the CTL (*solid red curve*) and its difference (*color*) from each sensitivity experiment over the central SCS. *Blue* (*brown*) *color* indicates that the positive vorticity in the CTL is larger (less) than that of the sensitivity experiment. *Left* (*right*) *vertical axis* is for precipitation (vorticity) if it is available. The wide *grey arrows* indicate the two northward marches of the subtropical front and the one retreat in between

The effect of the eastern IS forcing during FLOOD1 is negligible (Fig. 5c). However, it remarkably increases the rainfall over the YRB and South China when the subtropical front retreats in mid-July and moves northward again later during FLOOD2.

In contrast to the IS forcing through other LBs that has little influence on the SCS, the southern IS enhances the positive vorticity in late May over the SCS (Fig. 5d), evidencing that the southern IS forcing is responsible for triggering the EASM onset. The southern IS forcing also has a considerable contribution to increase the rainfall over South China and the YRB during the latter part of FLOOD2 (Fig. 4d).

In summary, the southern IS forcing triggers the SCS monsoon onset in late May. During FLOOD1, the western IS forcing dominates the propagation of the subtropical front and the associated extreme rainfall, while the northern IS forcing plays an auxiliary role. The IS forcing from the southern and eastern boundaries plays little role during FLOOD1. During FLOOD2, the eastern IS forcing plays a major role, but the western, northern, and southern IS forcing also contributes to the enhancement of the rainfall to various degrees. The southern IS forcing does not contribute to the retreat of the subtropical front back to the YRB.

7 Conclusion and discussion

The causes of the extremely heavy rainfall events during the EASM in 1998 were investigated with the PLF experiments using the regional climate model WRF. The PLF experiments were driven by the ensemble large-scale forcing in which three time scale variations were isolated from the climatology: SY, IS, and IA variations. The impact of the SY, IS, and the IA forcing through the lateral boundary on the seasonal-mean climate, the SCS monsoon onset, the migration of the subtropical front, and the extreme flooding events in the YRB and South China as well as heavy rainfall events in North China were assessed.

7.1 Conclusion

The external IS forcing not only triggers the monsoon onset over the SCS mainly through its southern boundary, but also drives two northward advances of the subtropical front and a southward retreat in between. The IS forcing also dominates the two extreme rainfall events over the YRB and South China.

The IS forcing has the largest contribution to the seasonal-mean rainfall anomalies over all three sub-regions of China. The SY forcing tends to have a moderate positive contribution to the YRB but significant negative contribution to the rainfall in South China. The IA forcing mainly enhances the rainfall in South China but reduces it slightly in the YRB. The IA forcing may also be responsible for the heavy rainfall over the Korean Peninsula.

During the first extreme event in June 1998, it is the IS forcing from the western boundary that drives the northward advance of the subtropical front and causes the associated heavy rainfall. The northern IS forcing also has a large contribution, whereas the contribution from the eastern and southern IS forcing is negligible. The IA forcing enhances the precipitation over both South China and the YRB.

During the second extreme event from mid-July to early August, it is the eastern IS forcing that drives the southward retreat and northward advance of the subtropical front and produces the intense rainfall. Each of the western, northern, and southern IS forcing contributes to the total effect of the IS forcing but their contributions are slightly less than that of the eastern IS forcing. The southern IS forcing don't contribute to the subtropical front retreat to the YRB. Both the SY forcing and IA forcing enhance the subtropical front and the associated precipitation during the second extreme event but are far less important than the IS forcing.

7.2 Discussion

Previous studies concluded that the northward propagating IS oscillation from the tropics regulates the extreme heavy rainfall during the EASM in 1998 (Wang et al. 2003; Zhu et al. 2003; Wang and Yang 2008). Here, we surprisingly find that the IS oscillation from the mid-latitude through the western, eastern and northern boundary, not that from the tropics (through the southern boundary), dominates the extreme rainfall events rather. This new modeling result supports the observational finding of Yang et al. (2010), which showed that both the high-frequency IS (bi-weekly) oscillation embeds in the mid-latitude jet stream and the low-frequency IS (30–60 day) oscillation associated with the westward extension of the WPSH, are major factors for the IS variation of rainfall in the Yangtze River Valley. The later may relate with a seesaw pattern between the tropics and subtropics (Lu et al. 2014).

The propagation of the IS oscillation is generally characterized by the movement of a cluster of cyclones and anticyclones. It is conceivable that the wet phase of the mid-latitude IS oscillation across the western boundary moves eastward and influences the dynamics of subtropical front when it encounters the southwesterly flow on the northwestern margin of the WPSH. The successive arrivals of such wet phases shift the rain band toward north as they are guided by the gradual northward shift of the jet stream in summer. That might be the mechanism of how the mid-latitude IS drives the northward advance of the subtropical front in the first extreme event in summer 1998. In the

second extreme event, after reestablishing the subtropical front over East China, the westward extension of the northwestern margin of the WPSH mainly regulates the northward movement of the subtropical front.

This study has some limitations. First, the lateral boundary forcing was linearly decomposed into multiple time-scale variations and the experimental results are also interpreted in terms of linear thinking. Yet, the atmospheric circulation is intrinsically nonlinear. However, our findings suggest that the linear decomposition and estimation may be valid to a large extent. In this regard, new numerical experiments could be designed to identify the nonlinear effects involved. Second, we only investigated the impacts of various time-scales forcing on the extreme events in summer 1998. In order to systematically uncover the essential effects of various forcing, multi-year simulations over multi-domain integrations are needed in the future. Last, even though we removed the SY variation from the lateral boundary forcing, we could not totally get rid of the influence of the SY variation because the local forcing and the model internal dynamics could generate SY perturbation inside the model domain. Thus, the nonlinear interaction among SY, IS, and IA variations in our model domain may be present in our results. However, these nonlinear behaviors may not be overwhelming; so our results remain useful in terms of identifying the effects of the forcing through the lateral boundary.

The regional models have been primarily used for downscaling studies of climate variability and prediction, as well as projection of forced future climate changes. Our PLF approach here opens a new avenue for application of the regional modeling to understand the impacts of various dynamical and physical processes on seasonal-mean and extreme climate anomalies. The PLF method used here can be applied to a broad range of phenomena in climate sciences.

Acknowledgments Both authors acknowledge the support from the APEC Climate Center (APCC). Bin Wang also acknowledges the support by the US NOAA ESS awards #NA13OAR4310167 and the National Research Foundation (NRF) of Korea through a Global Research Laboratory (GRL) grant of the Korean Ministry of Education, Science and Technology (MEST, #2011-0021927). This is Publication No. 19 of the Earth System Modeling Center.

References

Chang C-P (2004) East asian monsoon. World Scientific, Singapore

Chen L-T (2001) The role of the anomalous snow cover over the Qinghai-Xizang Plateau and ENSO in the great floods of 1998 in the Changjiang river valley. Chin J Atmos Sci 25:184–192

Ding Y-H (1994) Monsoons over China. Kluwer, Dordrecht

Ding Y-H, Liu Y-J (2001) Onset and the evolution of the summer monsoon over the South China Sea during SCSMEX field experiment in 1998. J Meteor Soc Jpn 79:255–276

Ding Y-H, Zhang Y, Ma Q, Hu G-Q (2001) Analysis of the large scale circulation features and synoptic systems in East Asia during the intensive observation period of GAME/HUBEX. J Meteorol Soc Jpn 79:277–300

Goswami BN, Wu G-X, Yasunari T (2006) The annual cycle, intraseasonal oscillations, and roadblock to seasonal predictability of the Asian summer monsoon. J Clim 19:5078–5099

Kanamitsu M, Ebisuzaki W, Woollen J, Yang S-K, Hnilo JJ, Fiorino M, Potter GL (2002) NCEP-DOE AMIP-II Reanalysis (R-2). Bull Am Meteor Soc 83:1631–1643

Lau N-C, Leetmaa A, Nath MJ, Wang H-L (2005) Influences of ENSO-Induced Indo-Western Pacific SST anomalies on extratropical atmospheric variability during the boreal summer. J Clim 18:2922–2942

Lu RY, Dong HL, Su Q, Ding H (2014) The 30–60-day intraseasonal oscillations over the subtropical western North Pacific during the summer of 1998. Adv Atmos Sci 31:1–7

McPhaden MJ (1999) Genesis and evolution of the 1997–98 El Niño. Science 283:950–954

NCC (National Climate Center of China) (1998) Heavy flooding and climate anomalies in China in 1998. China Meteorological Press, Beijing

Skamarock WC, Klemp JB, Dudhia J, Gill DO, Barker DM, Wang W, Powers JG (2005) A description of the advanced research WRF. NCAR technical note, NCAR/TN-468 + STR

Tao S-Y, Zhang Q-Y, Zhang S-L (1998) The great floods in the Changjiang river valley in 1998. Clim Environ Res 3:290–299

Uppala SM, Kallberg PW, Simmons AJ et al (2005) The ERA-40 reanalysis. Q J R Meteor Soc 131:2961–3012

Wang B (2006) The Asian monsoon. Springer, Berlin

Wang B, LinHo (2002) Rainy season of the Asian–Pacific summer monsoon. J Clim 15:386–398

Wang B, Yang H-W (2008) Hydrological issues in lateral boundary conditions for regional climate modeling: simulation of east asian summer monsoon in 1998. Clim Dyn 31:477–490

Wang B, Zhang Q (2002) Pacific-East Asian teleconnection, part II: how the Philippine Sea anticyclone established during development of El Nino. J Clim 15:3252–3265

Wang B, Wu R-G, Fu X-H (2000a) Pacific-East Asian teleconnection: how does ENSO affect East Asian climate? J Clim 13:1517–1536

Wang HJ, Matsuno T, Kurihara Y (2000b) Ensemble hindcast experiments for the flood period over China in 1998 by use of the CCSR/NIES atmospheric general circulation model. J Meteorol Soc Jpn 78:357–365

Wang Y-Q, Sen OL, Wang B (2003) A highly resolved regional climate model (IPRC-RegCM) and its simulation of the 1998 Severe Precipitation Event Over china. Part I: model description and verification of simulation. J Clim 16:1721–1738

Wang B, LinHo, Zhang Y-S, Lu M-M (2004) Definition of South China sea monsoon onset and commencement of the East Asia summer monsoon. J Clim 17:699–710

Yang J, Wang B, Wang B, Bao Q (2010) Biweekly and 21–30 day variabilities of the subtropical East Asian monsoon over the lower reach of Yangtze River Basin. J Clim 23:1146–1159

Yatagai A, Arakawa O, Kamiguchi K, Kawamoto H, Nodzu MI, Hamada A (2009) A 44-year daily gridded precipitation dataset for Asia based on a dense network of rain gauges. SOLA 5:137–140. doi:10.2151/sola.2009-035

Zhu C-W, Nakazawa T, Li J-P, Chen L-X (2003) The 30–60 day intraseasonal oscillation over the western North Pacific Ocean and its impacts on summer flooding in China during 1998. Geophys Res Lett. doi:10.1029/2003GL017817